THE SEISMOLOGICAL SOCIETY OF AMERICA
400 Evelyn Ave., Suite 201
Albany, CA 94706-1375
(510) 525-5474; FAX (510) 525-7204
www.seismosoc.org

Bulletin of the Seismological Society of America, Vol. 107, No. 2, pp. 521–531, April 2017, doi: 10.1785/0120150253

Ⓔ

Local Earthquake Magnitude Scale and *b*-Value for the Danakil Region of Northern Afar

by Finnigan Illsley-Kemp, Derek Keir,* Jonathan M. Bull, Atalay Ayele, James O. S. Hammond, J.-Michael Kendall, Ryan J. Gallacher, Thomas Gernon, and Berhe Goitom

Abstract The Danakil region of northern Afar is an area of ongoing seismic and volcanic activity caused by the final stages of continental breakup. To improve the quantification of seismicity, we developed a calibrated local earthquake magnitude scale. The accurate calculation of earthquake magnitudes allows the estimation of *b*-values and maximum magnitudes, both of which are essential for seismic-hazard analysis. Earthquake data collected between February 2011 and February 2013 on 11 three-component broadband seismometers were analyzed. A total of 4275 earthquakes were recorded over hypocentral distances ranging from 0 to 400 km. A total of 32,904 zero-to-peak amplitude measurements (A) were measured on the seismometer's horizontal components and were incorporated into a direct linear inversion that solved for all individual local earthquake magnitudes (M_L), 22 station correction factors (C), and 2 distance-dependent factors (n, K) in the equation $M_L = \log(A) - \log(A_0) + C$. The resultant distance correction term is given by $-\log(A_0) = 1.274336\log(r/17) - 0.000273(r - 17) + 2$. This distance correction term suggests that attenuation in the upper and mid-crust of northern Afar is relatively high, consistent with the presence of magmatic intrusions and partial melt. In contrast, attenuation in the lower crust and uppermost mantle is anomalously low, interpreted to be caused by a high melt fraction causing attenuation to occur outside the seismic frequency band. The calculated station corrections serve to reduce the M_L residuals significantly but do not show a correlation with regional geology. The cumulative seismicity rate produces a *b*-value of 0.9 ± 0.06, which is higher than most regions of continental rifting yet lower than values recorded at midocean ridges, further supporting the hypothesis that northern Afar is transitioning to seafloor spreading.

Electronic Supplement: List of all local earthquakes used in the study with calculated local magnitudes and associated magnitude error.

Introduction

The Danakil region, in northern Afar, is one of the few areas in the world where the transition from continental rifting to seafloor spreading is exposed subaerially. The region is seismically active and encompasses at least 24 active volcanic centers. The Ethiopian plateau, to the west of the Danakil depression, supports a significant population. Given its proximity to the western border fault of Afar, the town of Mekele faces a high level of seismic risk and experienced a swarm of earthquakes in 2002 (Ayele *et al.*, 2007). The accurate calculation of local magnitudes is a key component of seismic-hazard analysis, in particular when estimating *b*-values and maximum magnitudes. Accurate local magnitudes are also essential for studies that attempt to understand the geological processes occurring in locations such as northern Afar, for example, stress accumulation and amount of strain by faulting.

Seismic energy will attenuate at varying rates depending on factors such as temperature, composition, and fluid content of the crust as well as partial melt and magmatic intrusions (Schlotterbeck and Abers, 2001; Carletti and Gasperini, 2003; Keir *et al.*, 2006; Wang *et al.*, 2009). This rate of attenuation is characterized by an attenuation curve. The use of an inappropriate attenuation curve will result in errors when assigning local magnitude values to earthquakes.

*Also at the Dipartimento di Scienze della Terra, Università degli Studi di Firenze, Florence, Italy.

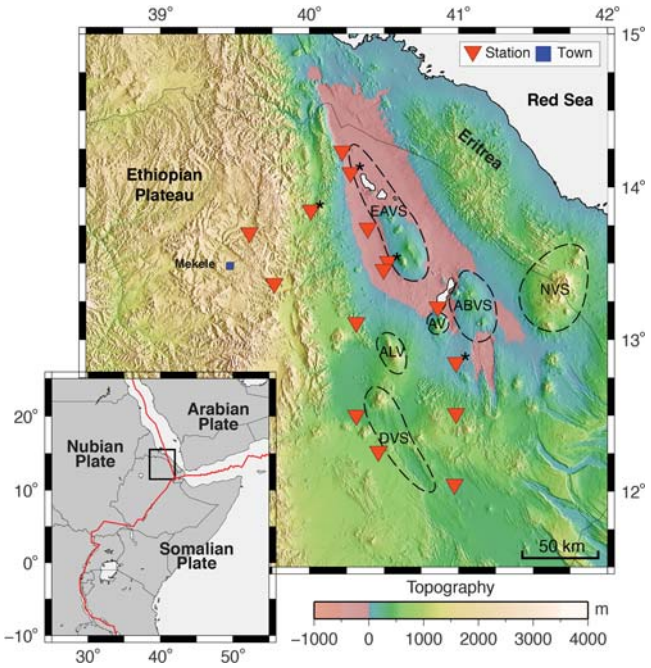

Figure 1. The seismic network deployed for this study. The network was in place between February 2011 and February 2013. Stations marked with asterisks had one or more faulty horizontal components and so were not used for calculating magnitudes. The region contains the Erta-Ale volcanic segment (EAVS), the Dabbahu volcanic segment (DVS), Nabro volcano (NVS), the Amarta-Barawli volcanic complex (ABVS), Afdera volcano (AV), and Alayta volcano (ALV). Topography data were taken from National Aeronautics and Space Administration (NASA)'s Shuttle Radar Topography Mission.

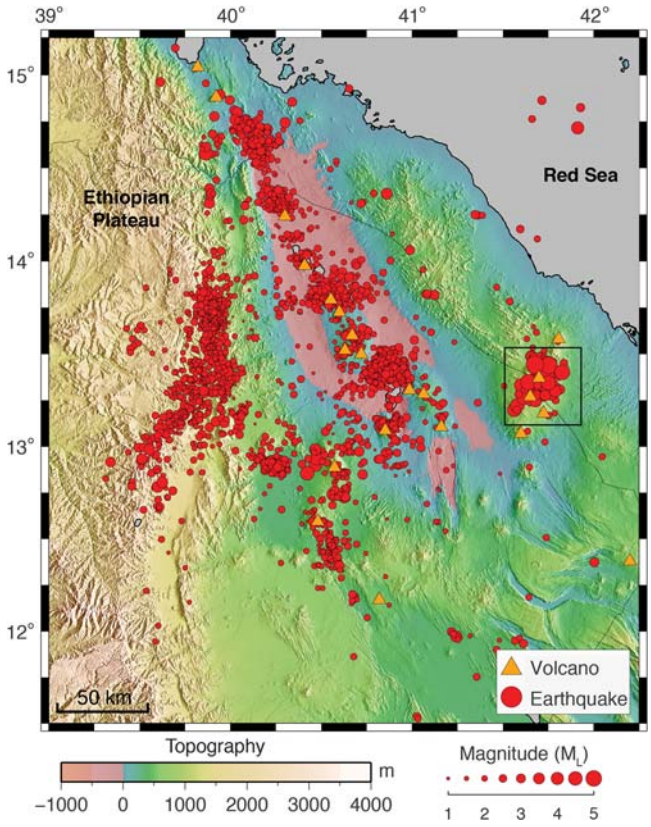

Figure 2. Locations and respective magnitudes of the 4275 earthquakes recorded in the two years between February 2011 and February 2013. All earthquakes have a minimum of four phases recorded on a minimum of three stations. The black box outlines those earthquakes associated with the eruption of Nabro volcano.

For two years, from 2011 to 2013, a seismic network was deployed over an area covering 260×150 km (Figs. 1 and 2). The goal of this study is to use the seismic data recorded by 11 broadband seismometers to quantify seismic activity including improved estimation of local magnitudes (M_L). To do this, we invert maximum body-wave amplitude and hypocentral distance information to derive a region-specific magnitude scale based on the definitions of Richter (1935, 1958).

Geological Setting

The Afar depression is a region that is in the late stages of continental breakup and lies at the triple junction between the Gulf of Aden, the southern Red Sea, and the Main Ethiopian rift (McKenzie and Davies, 1970; Mohr, 1970). The initiation of rifting in Afar occurred between 31 and 29 Ma (Hofmann *et al.*, 1997; Ukstins *et al.*, 2002), with initial extension thought to be accommodated by large-scale border faults (Wolfenden *et al.*, 2005). In northern Afar, strain localized to north-northwest–south-southeast (NNW–SSE)-trending 10–30-km-wide 60–100-km-long axial volcanic segments between 25 and 20 Ma (Hayward and Ebinger, 1996; Wolfenden *et al.*, 2005). Extension rates vary across the Danakil region, with extension of ~7 mm/yr in the northernmost area (15° N) and ~20 mm/yr in the south (13° N), with the extension directed east-northeast–west-southwest (McClusky *et al.*, 2010). The crust thins dramatically in the Danakil depression from ~27 km thickness in the rift to the south of the depression to <15 km beneath the depression (Makris and Ginzburg, 1987; Hammond *et al.*, 2011). The crust is >40 km thick beneath the Ethiopian plateau (Hammond *et al.*, 2011; Corti *et al.*, 2015).

The Danakil depression is an ~200-km long 50–150-km wide basin that is mostly below sea level but currently subaerial (Fig. 1). Because of the low elevation, the surface sediments in the area largely consist of thick layers of evaporites formed from repeated marine incursions (Barberi and Varet, 1970; Keir *et al.*, 2013), most recently 32,000 years ago (Bonatti *et al.*, 1971). The depression also contains the NNW–SSE-trending Erta-Ale volcanic segment (EAVS) and seven active volcanoes (Barberi and Varet, 1970; Nobile *et al.*, 2012; Fig. 1). The volcanic range is the focus for most of the magmatic activity in the region and is responsible for the majority of Quaternary to recent basalts in Afar (Bastow and Keir, 2011). It is also thought to mark the boundary of the Danakil microplate to the east (Eagles *et al.*, 2002). Geodetic observations of Gada-Ale, Dallol, and Alu-Dalafilla volcanoes in the Erta-Ale range have been successfully mod-

eled as fluxes of magma in upper-crustal reservoirs and intrusions (Amelung *et al.*, 2000; Field *et al.*, 2012; Nobile *et al.*, 2012; Pagli *et al.*, 2012).

In addition to the Erta-Ale volcanic range, there are a suite of other active volcanoes in the region (Fig. 1). At the southern edge of the Danakil depression, there are the Amarta-Barawli volcanic complex (ABVS), Afdera volcano (AV), and Alayta volcano (ALV) (Barberi and Varet, 1970). To the south of the Danakil depression in central west Afar, the rift axis steps en echelon to the southwest into the Dabbahu segment (DVS), which underwent a major dike intrusion episode during 2005–2010 (Wright *et al.*, 2006; Ebinger *et al.*, 2008; Barnie *et al.*, 2015). Nabro volcano (NVS), which erupted in June 2011, is on the eastern margin of the Danakil depression near the Eritrean–Ethiopian border (Hamlyn *et al.*, 2014; Goitom *et al.*, 2015; Fig. 1).

A variety of geophysical studies have shown that extension in Afar and the Main Ethiopian rift is accommodated by a combination of magmatic intrusion and lithospheric thinning (e.g., Bastow and Keir, 2011). There is extensive evidence, from Interferometric Synthetic Aperture Radar, magnetics, receiver functions, magnetotellurics, and seismic anisotropy for the presence of dikes and sills in the crust south of 13° N in Afar (Wright *et al.*, 2006; Keir *et al.*, 2011; Bridges *et al.*, 2012; Desissa *et al.*, 2013; Hammond, 2014). Furthermore, a study into 40 years of seismicity in Afar by Hofstetter and Beyth (2003) found that $>50\%$ of the geodetic moment, as predicted by plate separation rates, is taken up aseismically. Along with a larger body of work, these results show that magmatic processes play an important role in continental breakup (Calais *et al.*, 2008; Thybo and Nielsen, 2009). North of 13° N, in the Danakil depression, extensive crustal thinning is observed (Makris and Ginzburg, 1987; Hammond *et al.*, 2011). This suggests that ductile stretching and thinning of the crust may also play an important role in the accommodation of extension.

Many studies have attempted to investigate the thermochemical state of the mantle beneath Afar. Seismic tomography by Bastow *et al.* (2008) finds a broad low seismic-velocity structure beneath the Main Ethiopian rift that extends to depths of >400 km. Tomographic studies in northern Afar also show a region of low seismic velocity from 50 to 400 km depth, which is interpreted as a region of elevated temperature and partial melt (Hammond *et al.*, 2013; Stork *et al.*, 2013; Civiero *et al.*, 2015). This interpretation is further corroborated by modeling geochemical data that suggest an elevated mantle temperature of 1450° C (Ferguson *et al.*, 2013; Armitage *et al.*, 2015). The elevated mantle temperature will promote partial melting, even at relatively low rates of extension.

Data

The seismic network comprised 16 broadband seismometers that were operational for two years between February 2011 and February 2013 (Fig. 1). Thirteen Güralp CMG-3ESPCD instruments and three Güralp CMG-6TD instruments recorded continuous data at 50 Hz. A total of 4275 earthquakes were recorded across the network during the experiment and were located with HYPO2000 (Klein, 2002). We used a 1D velocity model based on a seismic refraction survey from the area (Makris and Ginzburg, 1987). Accounting for instrument faults, a total of 11 seismometers were used to calculate the local magnitude scale. The velocity seismograms were convolved with the standard Wood–Anderson response, with a Wood–Anderson gain of 2800, to produce Wood–Anderson displacement seismograms (Anderson and Wood, 1925; Kanamori and Jennings, 1978). The maximum peak-to-peak amplitude on both the east–west and the north–south components of each station was measured, in millimeters, for each event. The final dataset consisted of 32,904 amplitude measurements with hypocentral distances ranging from 0 to 420 km (Fig. 3).

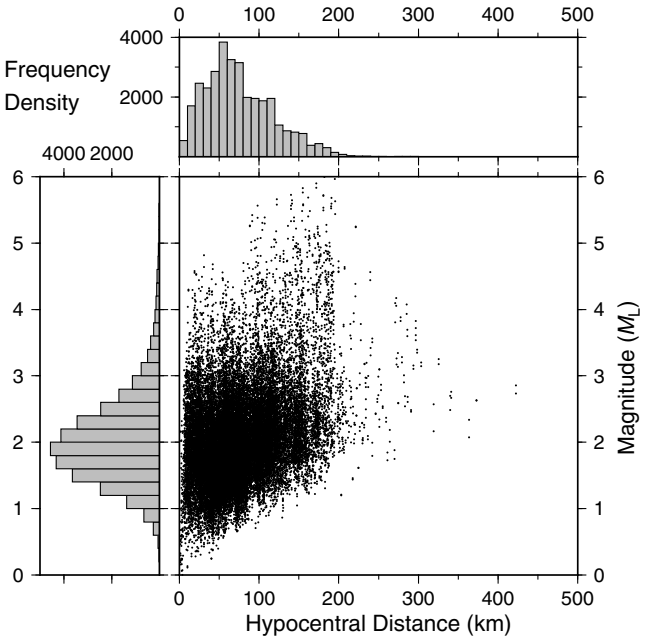

Figure 3. Magnitudes and hypocentral distances for the horizontal components for all stations. Magnitudes are calculated using the magnitude scale for the Danakil region.

Method

The definition of local magnitude M_L is given by Richter (1935, 1958):

$$M_L = \log(A) - \log(A_0) + C, \tag{1}$$

in which A is the maximum zero-to-peak amplitude on the horizontal seismogram, $\log(A_0)$ is a distance correction term that is calculated empirically, and C is a correction term for each component of each station that is also calculated empirically.

Richter originally defined the local magnitude scale such that an earthquake of M_L 3 would cause a 1 mm deflection on a standard horizontal Wood–Anderson seismograph at a distance of 100 km from the hypocenter. Hutton

and Boore (1987) observed that Richter's scale tended to underestimate magnitudes at stations close to the hypocenter and overestimate for more distant stations. To counter this problem, they developed a method to calculate how attenuation rates vary over increasing hypocentral distances, which yields an attenuation curve for specific regions. This allows for the magnitude scale to be normalized at a closer distance, thus minimizing geographical variations in wave propagation. They now define an M_L 3 earthquake as causing a 10 mm deflection on a Wood–Anderson seismograph at a distance of 17 km from the hypocenter. The distance correction term is defined as

$$-\log(A_0) = n\log(r/17) + K(r-17) + 2, \qquad (2)$$

in which n and K are constants to be calculated and relate to geometrical spreading and attenuation of seismic waves, respectively, and r is the hypocentral distance in kilometers.

Combining equations (1) and (2), the observed amplitude A_{ijk} for each component of each station for each event can be written as

$$\log(A_{ijk}) + 2 = -n\log(r_{ij}/17) - K(r_{ij}-17) + M_{L(i)} - C_{jk}, \qquad (3)$$

in which indexes i, j, and k represent events, stations, and components, respectively. It is now possible to invert for the unknowns n, K, M_L, and C. Each station has two correction terms associated with the north–south and east–west horizontal components. The set of equations includes a constraint that all station corrections sum to zero. The set of equations (3) can be combined into a matrix form, shown in equation (4), which represents a dot product equation $\mathbf{d} = \mathbf{m} \cdot \mathbf{A}$ and is a system of $N_e + 2N_s + 2$ unknowns, in which N_e and N_s are the number of events and stations, respectively. The data from Danakil include 4275 events recorded on 11 stations, producing a matrix with dimensions of $32{,}904 \times 4299$, with 4299 unknowns to be solved. Then, we solve equation (4) with a least-squares criterion and produce an optimal solution (Keir *et al.*, 2006). Our approach differs from many previous studies that have used an iterative technique (Langston *et al.*, 1998; Baumbach *et al.*, 2003). The direct inversion method is computationally much faster and has been tested by Pujol (2003) on data from Tanzania that was previously analyzed using the iterative technique (Langston *et al.*, 1998). The method used in this study has been tested on data from the Main Ethiopian rift and yielded identical results to those produced by Keir *et al.* (2006).

Results

The inversion produced an equation for the distance correction term $\log(A_0)$ for the Danakil region using a 17 km normalization

$$-\log(A_0) = 1.274336\log(r/17) - 0.0002731(r-17) + 2. \qquad (5)$$

Attenuation rates for the Danakil region (Fig. 4) are very similar to that of the Main Ethiopian rift for hypocentral distances up to ~70 km. For larger distances, the attenuation is significantly lower than in the Main Ethiopian rift (Keir *et al.*, 2006). The curve also shows that the attenuation rate in the Danakil region is significantly higher than in Tanzania (Langston *et al.*, 1998).

The effect that the newly derived attenuation curve has on magnitude estimates is shown in Figure 5. We show the magnitude residuals with increasing hypocentral distance when using the magnitude scale for the Danakil region, the Main Ethiopian rift (Keir *et al.*, 2006), and Tanzania (Langston *et al.*, 1998). Magnitude residuals calculated with the new Danakil magnitude scale display no bias with hypocentral distance, and hence an average residual of near zero at all hypocentral distances. In contrast, the Main Ethiopian rift scale overestimates magnitudes with increasing hypocentral distance, and the Tanzanian scale underestimates magnitudes, as shown by the respective gradients of the residual averages in Figure 5. The average variance of the residuals

$$\begin{pmatrix} \log(A_{111})+2 \\ \log(A_{112})+2 \\ \vdots \\ \log(A_{1N_s2})+2 \\ \log(A_{211})+2 \\ \vdots \\ \log(A_{N_eN_s2})+2 \end{pmatrix} = \begin{pmatrix} n \\ K \\ M_{L(1)} \\ M_{L(2)} \\ \vdots \\ M_{L(N_e)} \\ C_{11} \\ C_{12} \\ \vdots \\ C_{N_s2} \end{pmatrix} \cdot \begin{pmatrix} \log(r_{11}/17) & (r_{11}-17) & 1 & 0 & \cdots & 0 & 1 & 0 & \cdots & 0 \\ \log(r_{11}/17) & (r_{11}-17) & 1 & 0 & \cdots & 0 & 0 & 1 & \cdots & 0 \\ \vdots & \vdots & \vdots & \vdots & \ddots & \vdots & \vdots & \vdots & \ddots & \vdots \\ \log(r_{1N_s}/17) & (r_{1N_s}-17) & 1 & 0 & \cdots & 0 & 0 & 0 & \cdots & 1 \\ \log(r_{21}/17) & (r_{21}-17) & 0 & 1 & \cdots & 0 & 0 & 0 & \cdots & 1 \\ \vdots & \vdots & \vdots & \vdots & \ddots & \vdots & \vdots & \vdots & \ddots & \vdots \\ \log(r_{N_eN_s}/17) & (r_{N_eN_s}-17) & 0 & 0 & \cdots & 1 & 0 & 0 & \cdots & 1 \end{pmatrix} \qquad (4)$$

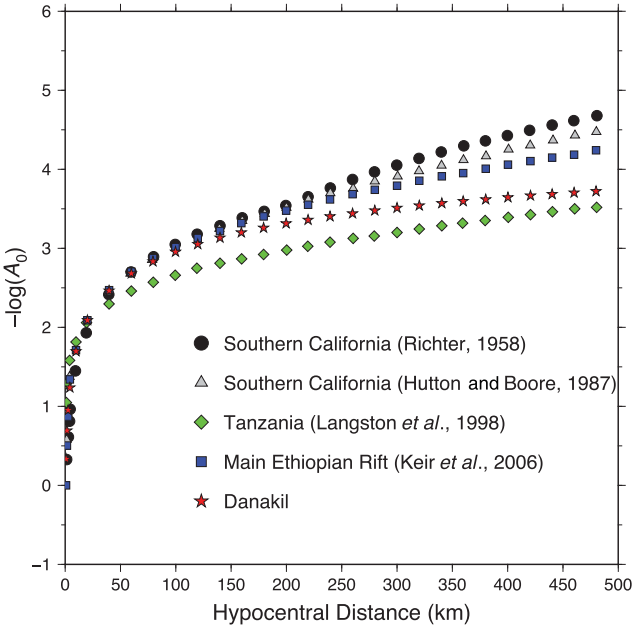

Figure 4. Comparison of attenuation curves for the Danakil region (this study), the Main Ethiopian rift (Keir *et al.*, 2006), Tanzania (Langston *et al.*, 1998), and southern California (Richter, 1958; Hutton and Boore, 1987). The attenuation rate in Danakil is significantly lower than that for the Main Ethiopian rift for hypocentral distances > 70 km.

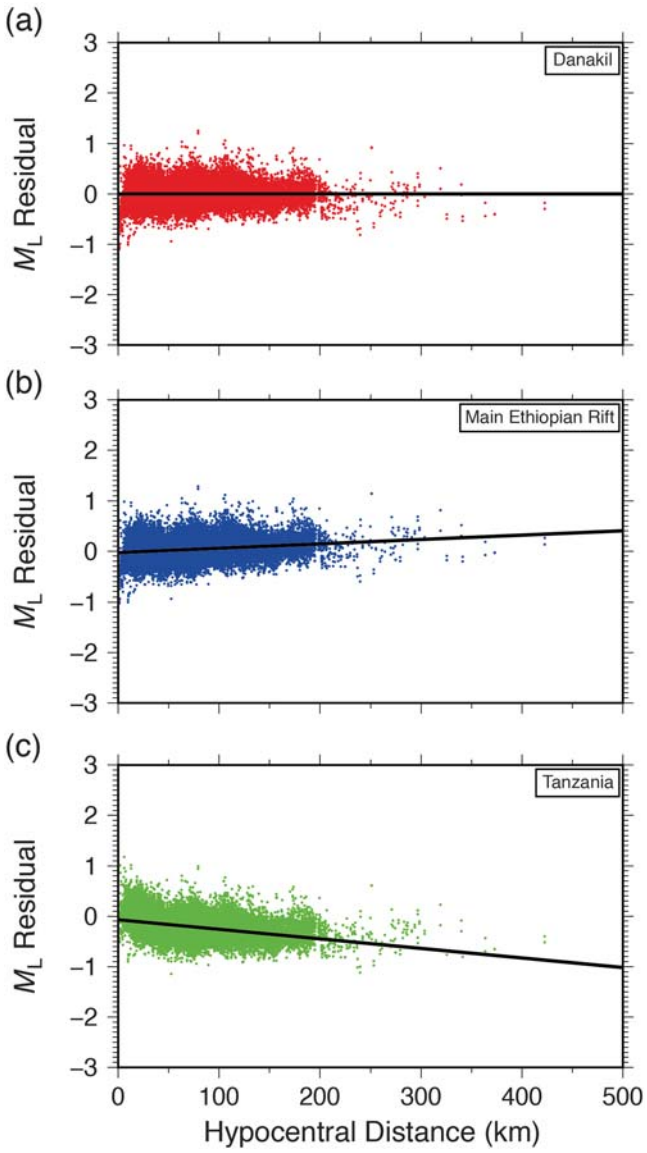

Figure 5. Magnitude residuals calculated for all events using three different scales; the newly derived magnitude scale for (a) Danakil, (b) the Main Ethiopian rift magnitude scale (Keir *et al.*, 2006), and (c) the Tanzania magnitude scale (Langston *et al.*, 1998). The Danakil magnitude scale minimizes residuals at all hypocentral distances, whereas the Main Ethiopian rift scale and the Tanzania scale overestimate and underestimate magnitudes, respectively.

for the Danakil magnitude scale is M_L 0.2; therefore the average error in magnitude calculation is given as $M_L \pm 0.2$. Individual magnitude errors for each event are listed in Ⓔ Tables S1 and S2, available in the electronic supplement to this article. To test whether the error in magnitude is dependent on magnitude value, we plot box plots of error values for events grouped at 0.5 magnitude intervals (Fig. 6). This clearly shows that magnitude error is stable for the full range of magnitudes in this study. As a further test of the magnitude scale, we compare Global Centroid Moment Tensor moment magnitudes (M_w) from the Danakil region with local magnitude values calculated with the derived magnitude scale (Table 1). The listed events are assumed to be representative, and worldwide comparisons of M_w and M_L find the two scales to be, on average, consistent for shallow earthquakes (< 33 km; Kanamori, 1983).

Station Corrections

The set of equation (4) includes a station correction term C_{jk} for each component of each station. There is also a condition included that all station corrections sum to zero. The station corrections calculated for the east–west components range from M_L 0.48 to −0.25 units, and the north–south-component corrections range from M_L 0.42 to −0.39 units (Fig. 7). Most stations have very similar station correction values for the north–south and east–west components. Through examining the distribution of station corrections, there is no obvious link between regional geology and station correction. It is therefore most likely that station correction values are dependent on very local effects, such as near-surface geology and the level of coupling between the seismometer and the soil.

Magnitude residuals, the magnitude calculated at a single station minus the average magnitude, were calculated at all stations for both the north–south and east–west components with and without station corrections (Fig. 8). Magnitude residuals calculated without station corrections have an average of almost zero ($M_L - 1.3 \times 10^{-2}$) and a variance of 0.096.

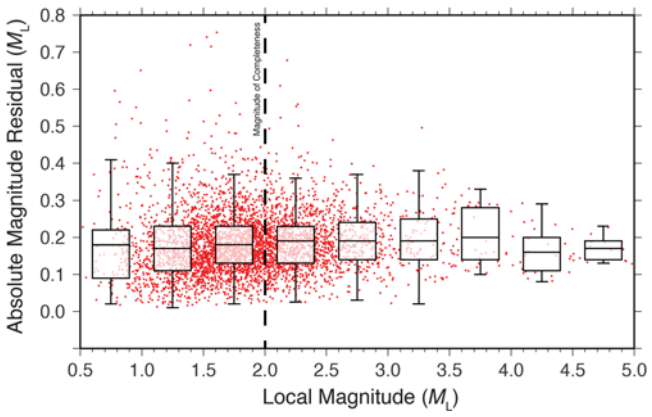

Figure 6. Box plot of magnitude error versus magnitude, binned in M_L 0.5 intervals. Box height represents the interquartile range, and whiskers represent extreme values that are within 1.5 interquartile range. Magnitude errors are clearly shown to be stable for the reported magnitude range.

Magnitude residuals calculated with station corrections included have an average of very nearly zero ($M_L - 3.3 \times 10^{-8}$) and a variance of 0.042. This shows that including the calculated station corrections brings the average residual closer to zero and reduces the variance by $>64\%$.

Discussion

We compare the attenuation curve derived for the Danakil region with those from other regions worldwide (Fig. 4). Attenuation is significantly higher in the Danakil region than in Tanzania for all hypocentral distances greater than 50 km (Langston *et al.*, 1998). The two regions are geologically very different; Tanzania is a region of early-stage nonvolcanic continental rifting of Archaean cratonic lithosphere. Archaean cratons generally consist of thick crystalline rock with very low geothermal gradients, both of which promote low seismic attenuation. The observed difference in seismic attenuation can therefore be explained by the presence of the Tanzanian craton.

Our new attenuation curve shows that at hypocentral distances of less than 100 km, the attenuation in Danakil is very similar to that in the Main Ethiopian rift and in southern California (Hutton and Boore, 1987; Keir *et al.*, 2006). High attenuation in southern California is explained by high geothermal gradients beneath the San Gabriel Mountains (Schlotterbeck and Abers, 2001). In the Main Ethiopian rift, the high rate of attenuation is ascribed to the presence of magmatic intrusions and partial melt within the crust (Keir *et al.*, 2006). The Danakil region has an abundance of active volcanism and a thinned crust that suggests the presence of partial melt and high geothermal gradients. These conditions can explain the high level of attenuation at hypocentral distances less than 100 km.

The attenuation rate in Danakil is significantly lower than that in the Main Ethiopian rift at hypocentral distances of over 100 km. Ray paths for earthquakes with hypocentral distances of over 100 and 150 km are shown in Figure 9. The rays at these hypocentral distances predominantly traverse from the Danakil depression in the north to the Dabbahu segment in the south. We then calculated 2D travel-time curves using *MacRay* (Luetgert, 1992) and a velocity model based on the seismic refraction survey by Makris and Ginzburg (1987), the results of which are shown in Figure 10. Earthquakes at these large hypocentral distances are sampling the lower crust and uppermost mantle at a maximum depth of ~45 km; therefore the low attenuation observed for the Danakil region is originating from these depths. A low attenuation rate could be consistent with a paucity of partial melt. However, previous geophysical work including high conductivity in magnetotelluric data and high V_P/V_S of >2 imaged by receiver functions strongly suggest that there is a large amount of melt present in the lower crust and uppermost mantle (Hammond *et al.*, 2011; Desissa *et al.*, 2013).

It is therefore unlikely that low attenuation is caused by low-melt fractions. Seismic attenuation in the upper mantle is thought to occur through two potential mechanisms: grain boundary sliding (Faul *et al.*, 2004) and melt squirt (Mavko and Nur, 1975; O'Connell and Budiansky, 1977). Grain boundary sliding has been shown to cause a broad absorption peak in the seismic frequency band and so cannot explain the low attenuation that we observe (Faul *et al.*, 2004). Hammond and Humphreys (2000) modeled the effect that melt squirt has on attenuation in the upper mantle with melt percentages ranging from 0% to 3%. They demonstrate that as

Table 1
A Comparison between Independently Calculated Moment Magnitudes (M_w) and Local Magnitudes (M_L)

Date (yyyy/mm/dd) and Time (hh:mm:ss)	Moment Magnitude M_w*	Local Magnitude M_L†	Depth (km)
2011/12/06 15:37:04	5.1	5.2	12
2011/12/06 19:21:50	5	5	1
2011/12/06 20:32:40	5.6	5.5	1
2011/12/06 21:03:23	5.4	5.7	2
2011/17/06 09:16:12	5.6	5.8	1

The events occurring on 12 June 2011 are associated with the eruption of Nabro volcano.
*Moment magnitude calculated by Global Centroid Moment Tensor and U.S. Geological Survey.
†Local magnitude calculated with local magnitude scale derived from this study.

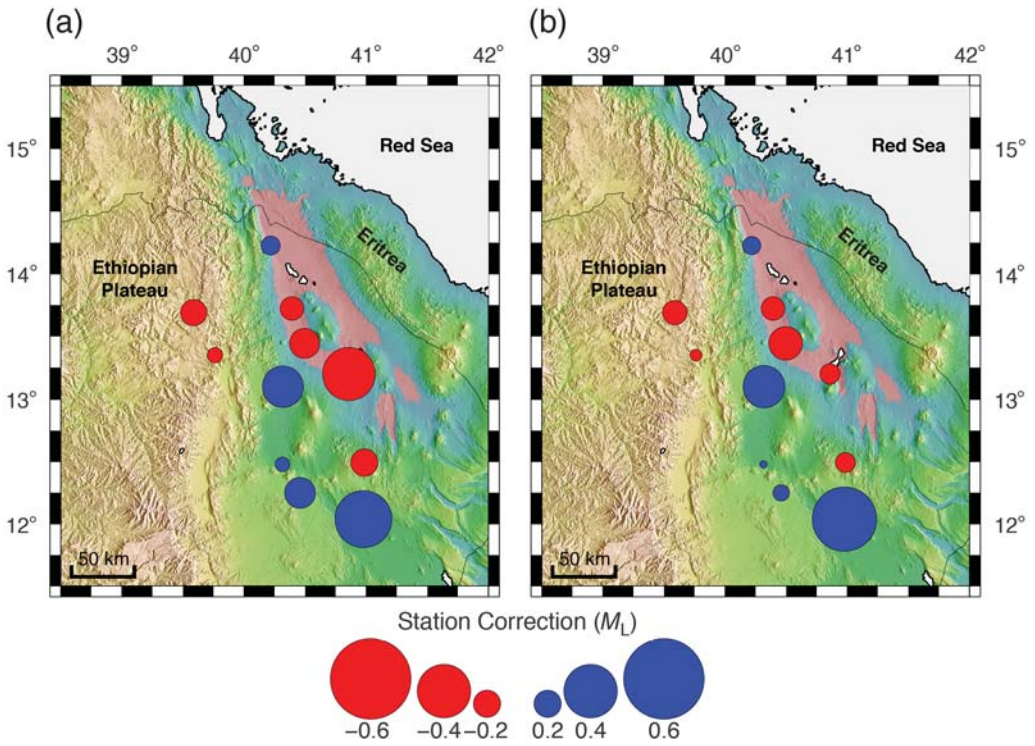

Figure 7. Variation of station corrections across the network. (a) North–south-component corrections. (b) East–west-component corrections. There is no clear correlation between regional geology and station correction. The corrections are therefore likely controlled by very local geology and site-specific variables.

melt percentage increases, melt pockets become more interconnected and melt squirt can occur at a faster rate. This has the effect of pushing the frequency at which attenuation occurs toward higher frequencies and away from the seismic frequency band. This interpretation of melt squirt causing low attenuation in the seismic frequency band has also been observed at the East Pacific Rise (Yang *et al.*, 2007). We suggest that the low attenuation observed in the uppermost mantle of Danakil can therefore be explained by a high melt fraction undergoing melt squirt.

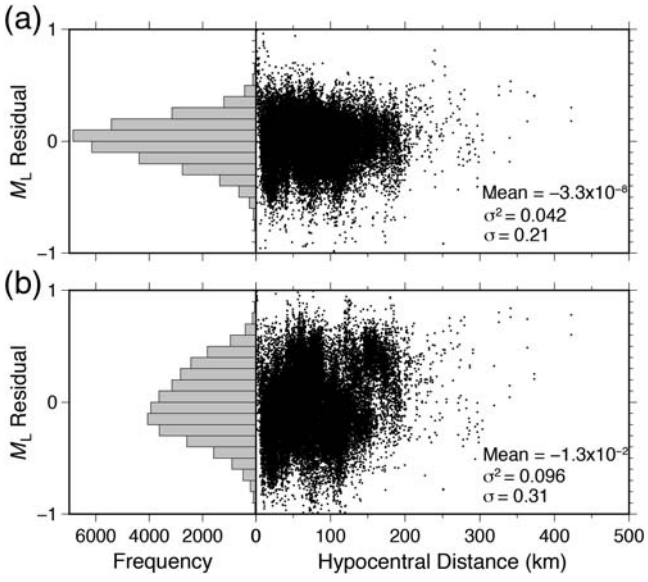

Figure 8. (a) Magnitude residuals calculated with station corrections. (b) Magnitude residuals calculated without station corrections. Magnitude residuals calculated with station corrections sum to nearly zero, and the variance (0.042) has been reduced by >64% when compared with the variance without station corrections (0.096).

We used the new magnitude scale for the Danakil region to investigate the seismicity that occurred in the region between February 2011 and February 2013. Figure 11 shows the Gutenberg–Richter distribution of log of the cumulative number of earthquakes of magnitude M_L or greater (Gutenberg and Richter, 1956). The time period of the study featured the eruption and associated seismic swarm of the Nabro volcano (Hamlyn *et al.*, 2014; Goitom *et al.*, 2015). Eruptions at caldera systems, such as Nabro, are extremely rare, and this was the first recorded eruption of the Nabro volcano. Because of the infrequent nature of the eruption, inclusion of the associated seismicity would bias the Gutenberg–Richter distribution. The events associated with the Nabro eruption have therefore been removed, based on their location at the volcano (latitude 13.1°–13.6°; longitude 41.5°–41.9°; Fig. 2). We estimate the magnitude of completeness by initially using the maximum curvature method (Wiemer and Wyss, 2000), which corresponds to the magnitude bin with the highest event frequency. In our data this is M_L 1.8 (Fig. 11). However, Woessner and Wiemer (2005) report that the maximum curvature method tends to under-

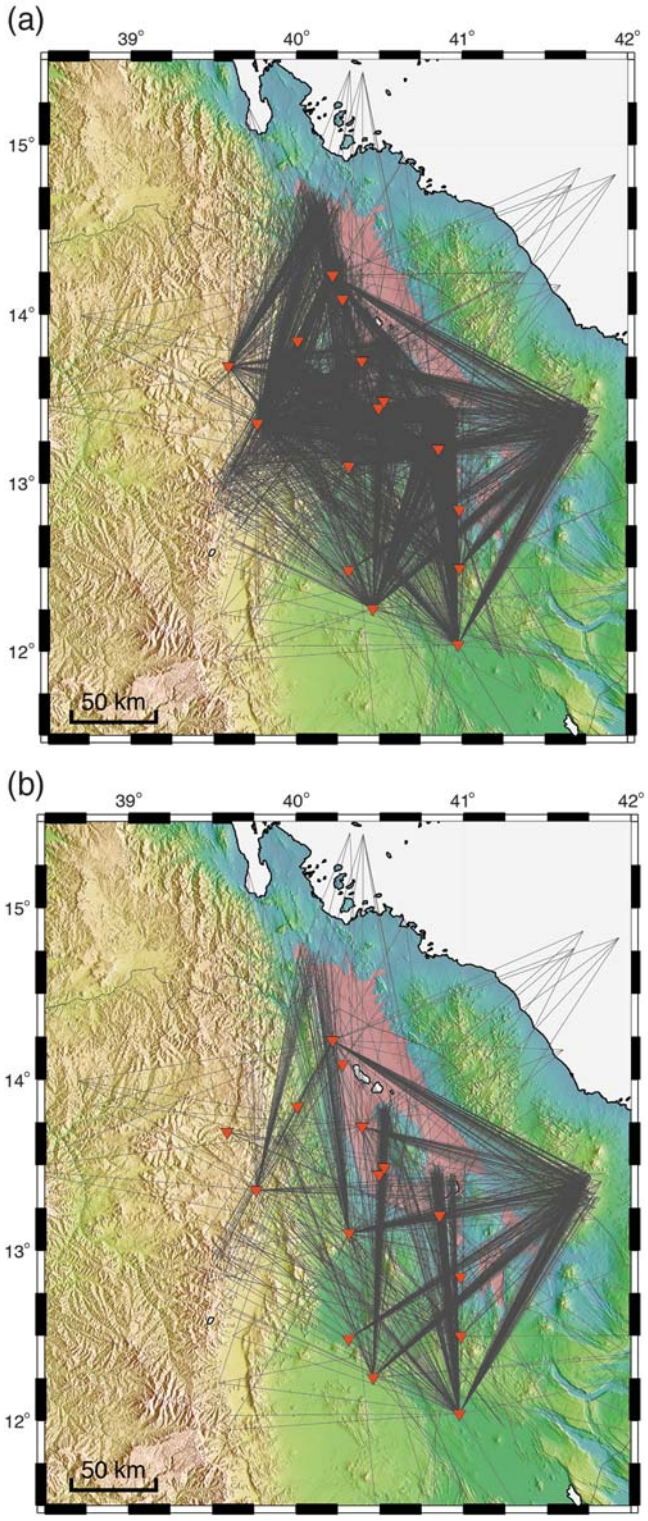

Figure 9. The ray paths for earthquakes with hypocentral distances over (a) 100 and (b) 150 km. The ray paths predominantly traverse the Danakil depression and Dabbahu segment region.

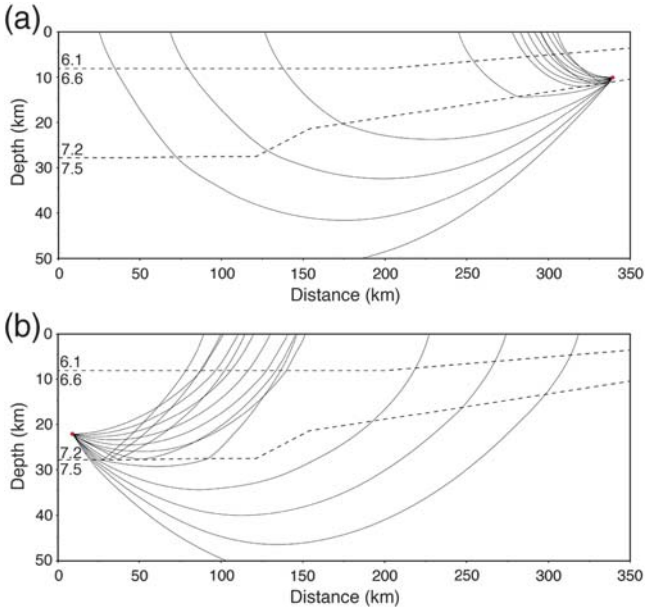

Figure 10. (a) Travel-time curves for an earthquake occurring in the north of the Danakil depression. The *S* waves sample the uppermost mantle at hypocentral distances >100 km, reaching depths of up to 40 km. (b) Travel-time curves for an earthquake occurring in the south of the study area. The *S* waves sample the uppermost mantle at hypocentral distances >125 km, reaching depths of up to 45 km. Layer *P*-wave velocities are given in km/s, taken from Makris and Ginzburg (1987).

estimate the magnitude of completeness by 0.1–0.2 magnitude units, and we therefore estimate a magnitude of completeness of M_L 2.0. A *b*-value of 0.9 was calculated using the maximum-likelihood calculation (Aki, 1965). We calculated an error of ± 0.06 by performing a bootstrap analysis following the method of Pickering *et al.* (1995). Including the events associated with the Nabro eruption in the *b*-value calculation reduces it to 0.8 ± 0.04. This is unsurprising given the number of large-magnitude events that occurred during the eruption. It is important to note that *b*-values have been observed to change significantly over small distances and through time, particularly in areas of volcanic activity (Wyss and McNutt, 1998; Barton *et al.*, 1999; Wyss *et al.*, 2001).

The Danakil region has a higher *b*-value than most other areas in the East African rift. South Sudan, Tanzania, and Kenya, which are all regions of continental rifting, have *b*-values that range from 0.7 to 0.9 (Tongue *et al.*, 1992; Ayele and Kulhanek, 1997; Langston *et al.*, 1998). The Danakil region *b*-value is also significantly higher than that in other continental rift systems, such as the Rio Grande and Eger rifts, both of which exhibit *b*-values of 0.8 (Ibs-von Seht *et al.*, 2008). In these regions, rifting is less developed and also less magmatically accommodated. A lack of magmatic activity during rifting allows greater stresses to accumulate in the crust, facilitating larger earthquakes and a lower *b*-value.

The *b*-value for Danakil is lower than values recorded at midocean ridges. At the Mid-Atlantic ridge, *b*-values have been observed to vary, but they are consistently above 1 and can reach values of up to 1.5 (Kong *et al.*, 1992; Barclay *et al.*, 2001; Tilmann *et al.*, 2004). Wilcock *et al.* (2002) performed a microearthquake study on the Endeavour segment of the Juan

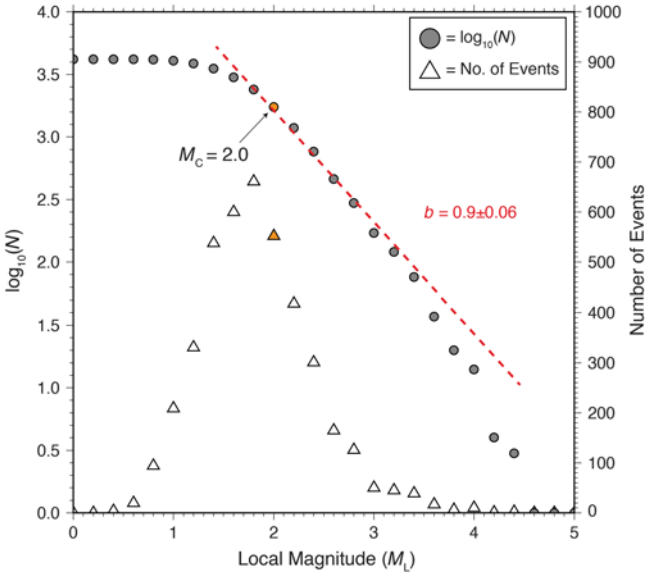

Figure 11. Analysis of earthquake magnitude distribution of earthquakes in the Danakil region, excluding those associated with the eruption of Nabro on 12 June 2011. (Left axis) Gutenberg–Richter distribution in which log(N) represents the log of the cumulative number of earthquakes of magnitude M_L or greater. (Right axis) Number of events represents the frequency of events in each magnitude bin. The magnitude of completeness (M_L 2.0) is calculated using the maximum curvature method (Wiemer and Wyss, 2000). We calculate the b-value using the maximum-likelihood method. The calculated b-value suggests that geodetic strain is primarily released through swarms of low-magnitude earthquakes, rather than large-scale faulting.

de Fuca ridge and recorded a b-value of 1.06. These b-values suggest that seismic energy at ocean ridges is primarily released through swarms of relatively low-magnitude earthquakes. The observation that the b-value for the Danakil region lies between those found at midocean ridges and at regions of continental rifting suggests that the Danakil region is at the transition from continental rifting to seafloor spreading.

The calculation of accurate local earthquake magnitudes is essential for estimating maximum magnitudes and for better quantification of time–space variations in seismicity b-values. As population grows in Afar and the Ethiopian plateau, more accurate quantification of earthquakes will aid seismic-hazard assessment in the region (e.g., Hagos *et al.*, 2006; Ayele *et al.*, 2007, 2015).

Conclusions

We calculated the first local magnitude scale for the Danakil region of northern Afar. The study used 32,904 amplitude measurements from 4275 earthquakes on 11 seismometers and yields the following equation:

$$-\log(A_0) = 1.274336\log(r/17) - 0.000273(r-17) + 2, \quad (6)$$

in which r is the hypocentral distance from station to earthquake. This equation and the corresponding attenuation curve show that the attenuation rate of seismic energy in Danakil is relatively high in the crust, consistent with the presence of magmatic intrusions and melt. The relatively low attenuation observed at greater depths could indicate a low melt percentage, inconsistent with independent geophysical data. We therefore suggest that the low attenuation rate is due to a sufficiently high melt fraction in the upper mantle beneath Danakil undergoing melt squirt and causing the seismic attenuation to occur outside the seismic frequency band.

We used the seismicity in Danakil to produce a Gutenberg–Richter relationship. The catalog is complete above M_L 2.0 and the calculated b-value is given as 0.9 ± 0.06. Our b-value is consistent with the area transitioning to seafloor spreading. Our improved magnitude scale and seismicity rate are critical for better quantification of seismic hazard. These results will also help quantify the distribution and amount of seismic strain.

Data and Resources

Seismograms used in this study were collected as part of the Afar0911 experiment using Seismic Equipment Infrastructure in the UK (SEIS-UK) instruments. We provide the catalog of earthquakes used in this study in the electronic supplement to this article. Plots were made using the Generic Mapping Tools v. 4.5.8 (www.soest.hawaii.edu/gmt, last accessed September 2015; Wessel and Smith, 1998).

Acknowledgments

We thank Seismic Equipment Infrastructure in the UK (SEIS-UK) for use of the instruments and their computing facilities. The facilities of SEIS-UK are supported by the Natural Environment Research Council (NERC) under Agreement R8/H10/64. F. I.-K. is funded through NERC studentship NE/L002531/1 and a grant to Graduate School of the National Oceanography Centre of Southampton (GSNOCS) from Roy Franklin O.B.E. D. K. is supported by NERC Grant Number NE/L013932. Funding for fieldwork is from BHP Billiton. We also acknowledge assistance from Addis Ababa University and the Afar National Regional State Government. We would like to thank Yavor Kamer and an anonymous reviewer for constructive reviews of the article.

References

Aki, K. (1965). Maximum likelihood estimate of b in the formula $\log N = a - bM$ and its confidence limits, *Bull. Earthq. Res. Inst.* **43,** 237–239.

Amelung, F., C. Oppenheimer, P. Segall, and H. Zebker (2000). Ground deformation near Gada 'Ale Volcano, Afar, observed by radar interferometry, *Geophys. Res. Lett.* **27,** no. 19, 3093–3096.

Anderson, J., and H. O. Wood (1925). Description and theory of the torsion seismometer, *Bull. Seismol. Soc. Am.* **15,** no. 1, 1–72.

Armitage, J. J., D. J. Ferguson, S. Goes, J. O. S. Hammond, E. Calais, C. A. Rychert, and N. Harmon (2015). Upper mantle temperature and the onset of extension and break-up in Afar, Africa, *Earth Planet. Sci. Lett.* **418,** 78–90.

Ayele, A., and O. Kulhanek (1997). Spatial and temporal variation of seismicity in the Horn of Africa from 1960 to 1993, *Geophys. J. Int.* **130,** 805–810.

Ayele, A., C. J. Ebinger, C. van Alstyne, D. Keir, C. W. Nixon, M. Belachew, and J. O. S. Hammond (2015). Seismicity of the central Afar rift and implications for Tendaho dam hazards, *Geol. Soc. Spec. Pub.* **420,** doi: 10.1144/SP420.9.

Ayele, A., G. Stuart, I. Bastow, and D. Keir (2007). The August 2002 earthquake sequence in north Afar: Insights into the neotectonics of the Danakil microplate, *J. Afr. Earth Sci.* **40,** 70–79.

Barberi, F., and J. Varet (1970). The Erta Ale volcanic range (Danakil depression, northern Afar, Ethiopia), *Bull. Volcanol.* **34,** no. 4, 848–917.

Barclay, A. H., D. R. Toomey, and S. C. Solomon (2001). Microearthquake characteristics and crustal V_p/V_s structure at the Mid-Atlantic Ridge, 35 N, *J. Geophys. Res.* **106,** no. B2, 2017–2034.

Barnie, T. D., D. Keir, I. Hamling, B. Hofmann, M. Belachew, S. Carn, D. Eastwell, J. O. S. Hammond, A. Ayele, C. Oppenheimer, *et al.* (2015). A multidisciplinary study of the final episode of the Manda Hararo dyke sequence, Ethiopia, and implications for trends in volcanism during the rifting cycle, *Geol. Soc. Lond.* **420,** doi: 10.1144/SP420.6.

Barton, D., G. Foulger, J. Henderson, and B. Julian (1999). Frequency–magnitude statistics and spatial correlation dimensions of earthquakes at Long Valley caldera, California, *Geophys. J. Int.* **138,** no. 2, 563–570.

Bastow, I., and D. Keir (2011). The protracted development of the continent-ocean transition in Afar, *Nat. Geosci.* **4,** 248–250.

Bastow, I., A. Nyblade, G. Stuart, T. Rooney, and M. Benoit (2008). Upper mantle seismic structure beneath the Ethiopian hotspot: Rifting at the edge of the African low velocity anomaly, *Geochem. Geophys. Geosyst.* **9,** no. 12, doi: 10.1029/2008GC002107.

Baumbach, M., D. Bindi, H. Grosser, C. Milkereit, S. Parolai, R. Wang, S. Karakisa, S. Zünbül, and J. Zschau (2003). Calibration of an M_L scale in northwestern Turkey from 1999 Izmit aftershocks, *Bull. Seismol. Soc. Am.* **93,** no. 5, 2289–2295.

Bonatti, E., C. Emiliani, G. Ostlund, and H. Rydell (1971). Final desiccation of the Afar rift, Ethiopia, *Science* **172,** no. 3982, 468–469.

Bridges, D., K. Mickus, S. Gao, M. Abdelsalam, and A. Alemu (2012). Magnetic stripes of a transitional continental rift in Afar, *Geology* **40,** no. 3, 203–206.

Calais, E., N. d'Oreye, J. Albaric, A. Deschamps, D. Delvaux, J. Déverchere, C. Ebinger, R. W. Ferdinand, F. Kervyn, A. S. Macheyeki, *et al.* (2008). Strain accommodation by slow slip and dyking in a youthful continental rift, East Africa, *Nature* **456,** 783–787.

Carletti, F., and P. Gasperini (2003). Lateral variations of seismic intensity attenuation in Italy, *Geophys. J. Int.* **155,** no. 3, 839–856.

Civiero, C., J. O. S. Hammond, S. Goes, S. Fishwick, A. Ahmed, A. Ayele, C. Doubre, B. Goitom, D. Keir, J-M. Kendall, *et al.* (2015). Multiple mantle upwellings in the transition zone beneath the northern East African Rift System from relative P wave travel time tomography, *Geochem. Geophys. Geosyst.* **16,** no. 9, 2949–2968.

Corti, G., A. Agostini, D. Keir, J. Van Wijk, I. D. Bastow, and G. Ranalli (2015). Magma-induced axial subsidence during final-stage rifting: Implications for the development of seaward-dipping reflectors, *Geosphere* **11,** no. 3, 563–571.

Desissa, M., N. Johnson, K. Whaler, S. Hautot, S. Fisseha, and G. Dawes (2013). A mantle magma reservoir beneath an incipient mid-ocean ridge in Afar, Ethiopia, *Nat. Geosci.* **6,** no. 10, 861–865.

Eagles, G., R. Gloaguen, and C. Ebinger (2002). Kinematics of the Danakil microplate, *Earth Planet. Sci. Lett.* **203,** 607–620.

Ebinger, C. J., D. Keir, A. Ayele, E. Calais, T. J. Wright, M. Belachew, J. O. S. Hammond, E. Campbell, and W. Buck (2008). Capturing magma intrusion and faulting processes during continental rupture: Seismicity of the Dabbahu (Afar) rift, *Geophys. J. Int.* **174,** no. 3, 1138–1152, doi: 10.1111/j.1365-246X.2008.03877.x.

Faul, U. H., J. D. Fitz Gerald, and I. Jackson (2004). Shear wave attenuation and dispersion in melt-bearing olivine polycrystals: 2. Microstructural interpretation and seismological implications, *J. Geophys. Res.* **109,** no. B6, doi: 10.1029/2003JB002407.

Ferguson, D. J., J. Maclennan, I. Bastow, D. Pyle, S. Jones, D. Keir, J. Blundy, T. Plank, and G. Yirgu (2013). Melting during late-stage rifting in Afar is hot and deep, *Nature* **499,** no. 7456, 70–73.

Field, L., T. Barnie, J. Blundy, R. A. Brooker, D. Keir, E. Lewi, and K. Saunders (2012). Integrated field, satellite and petrological observations of the November 2010 eruption of Erta Ale, *Bull. Volcanol.* **74,** no. 10, 2251–2271.

Goitom, B., C. Oppenheimer, J. O. S. Hammond, R. Grandin, T. Barnie, A. Donovan, G. Ogubazghi, E. Yohannes, G. Kibrom, J.-M. Kendall, *et al.* (2015). First recorded eruption of Nabro volcano, Eritrea, 2011, *Bull. Volcanol.* **77,** no. 10, 1–21.

Gutenberg, B., and C. F. Richter (1956). Earthquake magnitude, inten sity, energy, and acceleration, *Bull. Seismol. Soc. Am.* **46,** no. 2, 105–145.

Hagos, L., R. Arvidsson, and R. Roberts (2006). Application of the spatially smoothed seismicity and Monte Carlo methods to estimate the seismic hazard of Eritrea and the surrounding region, *Nat. Hazards* **39,** no. 3, 395–418.

Hamlyn, J. E., D. Keir, T. J. Wright, J. W. Neuberg, B. Goitom, J. O. S. Hammond, C. Pagli, C. Oppenheimer, J. Kendall, and R. Grandin (2014). Seismicity and subsidence following the 2011 Nabro eruption, Eritrea: Insights into the plumbing system of an off-rift volcano, *J. Geophys. Res.* **119,** no. 11, 8267–8282.

Hammond, J. O. S. (2014). Constraining melt geometries beneath the Afar Depression, Ethiopia from teleseismic receiver functions: The anisotropic H-κ stacking technique, *Geochem. Geophys. Geosyst.* **15,** no. 4, 1316–1332.

Hammond, J. O. S., J.-M. Kendall, G. Stuart, C. Ebinger, I. Bastow, D. Keir, A. Ayele, M. Belachew, B. Goitom, G. Ogubazghi, *et al.* (2013). Mantle upwelling and initiation of rift segmentation beneath the Afar Depression, *Geology* **41,** no. 6, 635–638.

Hammond, J. O. S., J.-M. Kendall, G. Stuart, D. Keir, C. Ebinger, A. Ayele, and M. Belachew (2011). The nature of the crust beneath the Afar triple junction: Evidence from receiver functions, *Geochem. Geophys. Geosyst.* **12,** no. 12.

Hammond, W. C., and E. D. Humphreys (2000). Upper mantle seismic wave attenuation—Effects of realistic partial melt distribution, *J. Geophys. Res.* **105,** 10,987–10,999.

Hayward, N., and C. Ebinger (1996). Variations in the along–axis segmentation of the Afar rift system, *Tectonics* **15,** 244–257.

Hofmann, C., V. Courtillot, G. Feraud, P. Rochette, G. Yirgu, E. Ketefo, and R. Pik (1997). Timing of the Ethiopian flood basalt event and implications for plume birth and global change, *Nature* **389,** 838–841.

Hofstetter, R., and M. Beyth (2003). The Afar depression: Interpretation of the 1960–2000 earthquakes, *Geophys. J. Int.* **155,** no. 2, 715–732.

Hutton, L., and D. M. Boore (1987). The M_L scale in southern California, *Bull. Seismol. Soc. Am.* **77,** no. 6, 2074–2094.

Ibs-von Seht, M., T. Plenefisch, and K. Klinge (2008). Earthquake swarms in continental rifts—A comparison of selected cases in America, Africa and Europe, *Tectonophysics* **452,** no. 1, 66–77.

Kanamori, H. (1983). Magnitude scale and quantification of earthquakes, *Tectonophysics* **93,** no. 3, 185–199.

Kanamori, H., and P. C. Jennings (1978). Determination of local magnitude, M_L, from strong-motion accelerograms, *Bull. Seismol. Soc. Am.* **68,** no. 2, 471–485.

Keir, D., I. D. Bastow, C. Pagli, and E. L. Chambers (2013). The development of extension and magmatism in the Red Sea rift of Afar, *Tectonophysics* **607,** 98–114.

Keir, D., M. Belachew, C. Ebinger, J.-M. Kendall, J. O. S. Hammond, G. W. Stuart, A. Ayele, and J. Rowland (2011). Mapping the evolving strain field during continental breakup from crustal anisotropy in the Afar Depression, *Nat. Commun.* **2,** 285.

Keir, D., G. Stuart, A. Jackson, and A. Ayele (2006). Local earthquake magnitude scale and seismicity rate for the Ethiopian rift, *Bull. Seismol. Soc. Am.* **96,** no. 6, 2221–2230.

Klein, F. (2002). User's guide to HYPOINVERSE-2000: A Fortran program to solve for earthquake locations and magnitudes, *U.S. Geol. Surv. Open File Rept. 02–171*.

Kong, L. S., S. C. Solomon, and G. Purdy (1992). Microearthquake characteristics of a mid-ocean ridge along-axis high, *J. Geophys. Res.* **97,** no. B2, 1659–1685.

Langston, C. A., R. Brazier, A. A. Nyblade, and T. J. Owens (1998). Local magnitude scale and seismicity rate for Tanzania, East Africa, *Bull. Seismol. Soc. Am.* **88,** no. 3, 712–721.

Luetgert, J. H. (1992). MacRay; Interactive two-dimensional seismic raytracing for the Macintosh, *U.S. Geol. Surv. Tech. Rept.; Books and Open-File Reports Section 92-356*.

Makris, J., and A. Ginzburg (1987). The Afar depression: Transition between continental rifting and sea-floor spreading, *Tectonophysics* **141,** 199–214.

Mavko, G., and A. Nur (1975). Melt squirt in the asthenosphere, *J. Geophys. Res.* **80,** no. 11, 1444–1448.

McClusky, S., R. Reilinger, G. Ogubazghi, A. Amleson, B. Healeb, P. Vernant, J. Sholan, S. Fisseha, L. Asfaw, R. Bendick, *et al.* (2010). Kinematics of the southern Red Sea–Afar Triple Junction and implications for plate dynamics, *Geophys. Res. Lett.* **37,** no. 5.

McKenzie, D., and D. Davies (1970). Plate tectonics of the Red Sea and east Africa, *Nature* **226,** 243–248.

Mohr, P. (1970). The Afar Triple Junction and sea-floor spreading, *J. Geophys. Res.* **75,** no. 35, 7340–7352.

Nobile, A., C. Pagli, D. Keir, T. J. Wright, A. Ayele, J. Ruch, and V. Acocella (2012). Dike-fault interaction during the 2004 Dallol intrusion at the northern edge of the Erta Ale Ridge (Afar, Ethiopia), *Geophys. Res. Lett.* **39,** no. 19.

O'Connell, R. J., and B. Budiansky (1977). Viscoelastic properties of fluid-saturated cracked solids, *J. Geophys. Res.* **82,** no. 36, 5719–5735.

Pagli, C., T. J. Wright, C. J. Ebinger, S.-H. Yun, J. R. Cann, T. Barnie, and A. Ayele (2012). Shallow axial magma chamber at the slow-spreading Erta Ale Ridge, *Nat. Geosci.* **5,** no. 4, 284–288.

Pickering, G., J. Bull, and D. Sanderson (1995). Sampling power-law distributions, *Tectonophysics* **248,** no. 1, 1–20.

Pujol, J. (2003). Determination of a local magnitude scale: A generalized inverse solution, *Bull. Seismol. Soc. Am.* **93,** no. 6, 2758–2761.

Richter, C. F. (1935). An instrumental earthquake magnitude scale, *Bull. Seismol. Soc. Am.* **25,** no. 1, 1–32.

Richter, C. F. (1958). *Elementary Seismology*, W. H. Freeman, New York, New York.

Schlotterbeck, B. A., and G. A. Abers (2001). Three-dimensional attenuation variations in southern California, *J. Geophys. Res.* **106,** no. B12, 30,719–30,735.

Stork, A., G. Stuart, C. Henderson, D. Keir, and J. O. S. Hammond (2013). Uppermost mantle (*Pn*) velocity model for the Afar region, Ethiopia: An insight into rifting processes, *Geophys. J. Int.* **193,** no. 1, 321–328.

Thybo, H., and C. Nielsen (2009). Magma-compensated crustal thinning in continental rift zones, *Nature* **457,** 873–876.

Tilmann, F., E. Flueh, L. Planert, T. Reston, and W. Weinrebe (2004). Micro-earthquake seismicity of the Mid-Atlantic Ridge at 5° S: A view of tectonic extension, *J. Geophys. Res.* **109,** no. B6.

Tongue, J., P. Maguire, and P. Young (1992). Seismicity distribution from temporary earthquake recording networks in Kenya, *Tectonophysics* **204,** no. 1, 71–79.

Ukstins, I., P. Renne, E. Wolfenden, J. Baker, D. Ayalew, and M. Menzies (2002). Matching conjugate volcanic rifted margins: $^{40}Ar/^{30}Ar$ chrono stratigraphy of pre- and syn-rift bimodal flood volcanism in Ethiopia and Yemen, *Earth Planet. Sci. Lett.* **198,** 289–306.

Wang, Y., D. Forsyth, and B. Savage (2009). Convective upwelling in the mantle beneath the Gulf of California, *Nature* **462,** 499–501.

Wessel, P., and W. H. Smith (1998). New, improved version of generic mapping tools released, *Eos Trans. AGU* **79,** 579.

Wiemer, S., and M. Wyss (2000). Minimum magnitude of completeness in earthquake catalogs: Examples from Alaska, the western United States, and Japan, *Bull. Seismol. Soc. Am.* **90,** no. 4, 859–869.

Wilcock, W. S., S. D. Archer, and G. Purdy (2002). Microearthquakes on the Endeavour segment of the Juan de Fuca Ridge, *J. Geophys. Res.* **107,** no. B12, EPM 4-1–EPM 4-21.

Woessner, J., and S. Wiemer (2005). Assessing the quality of earthquake catalogues: Estimating the magnitude of completeness and its uncertainty, *Bull. Seismol. Soc. Am.* **95,** no. 2, 684–698.

Wolfenden, E., C. Ebinger, G. Yirgu, P. Renne, and S. Kelley (2005). Evolution of a volcanic rifted margin: Southern Red Sea, Ethiopia, *Bull. Geol. Soc. Am.* **117,** nos. 7/8, 846–864.

Wright, T., C. Ebinger, J. Biggs, A. Ayele, G. Yirgu, D. Keir, and A. Stork (2006). Magma-maintained rift segmentation at continental rupture in the 2005 Afar dyking episode, *Nature* **442,** no. 7100, 291–294.

Wyss, M., and S. R. McNutt (1998). Temporal and three-dimensional spatial analyses of the frequency–magnitude distribution near Long Valley Caldera, California, *Geophys. J. Int.* **134,** no. 2, 409–421.

Wyss, M., F. Klein, K. Nagamine, and S. Wiemer (2001). Anomalously high b-values in the South Flank of Kilauea volcano, Hawaii: Evidence for the distribution of magma below Kilauea's East rift zone, *J. Volcanol. Geoth. Res.* **106,** no. 1, 23–37.

Yang, Y., D. W. Forsyth, and D. S. Weeraratne (2007). Seismic attenuation near the East Pacific Rise and the origin of the low-velocity zone, *Earth Planet. Sci. Lett.* **258,** no. 1, 260–268.

Ocean and Earth Science
National Oceanography Centre Southampton
University of Southampton
Southampton SO14 3ZH, United Kingdom
F.Illsley-Kemp@soton.ac.uk
D.Keir@soton.ac.uk
bull@noc.soton.ac.uk
R.Gallacher@soton.ac.uk
Thomas.Gernon@noc.soton.ac.uk
(F.I.-K., D.K., J.M.B., R.J.G., T.G.)

Institute of Geophysics Space Science and Astronomy
Addis Ababa University
King George VI Street
Addis Ababa 1000, Ethiopia
atalay.ayele@aau.edu.et
(A.A.)

Department of Earth and Planetary Sciences, Birkbeck
University of London
Malet Street
London WC1E 7HX, United Kingdom
j.hammond@ucl.ac.uk
(J.O.S.H.)

School of Earth Sciences
University of Bristol
Bristol BS8 1RJ, United Kingdom
gljmk@bristol.ac.uk
bg12363@bristol.ac.uk
(J.-M.K., B.G.)

Manuscript received 15 September 2015;
Published Online 24 January 2017